TECHNICAL ARTICLE

From Prussian blue to iron carbides: high-temperature XRD monitoring of thermal transformation under inert gases

Claudia Aparicio,[a] Jan Filip, and Libor Machala
Regional Centre of Advanced Technologies and Materials, Faculty of Science, Palacký University, Šlechtitelů 27, 783 71 Olomouc, Czech Republic

(Received 16 October 2016; accepted 5 April 2017)

The thermal behavior and decomposition reaction of Prussian blue (PB) ($Fe_4^{3+}[Fe^{2+}(CN)_6]_3 \cdot xH_2O$) was studied under inert atmosphere of argon by simultaneous thermogravimetry and differential scanning calorimetry, from room temperature up to 900 °C, with a heating rate of 5 K min^{-1}. Parallel to the thermogravimetric measurements, the thermal process was monitored by *in situ* X-ray powder diffraction (XRD) technique under nitrogen atmosphere. The thermogravimetric data show six steps, corresponding to different stages of the decomposition reaction; comparable results are also obtained by *in situ* XRD. In addition, a set of PB samples heated up to selected temperatures (190, 300, 370, 540, 680, and 790 °C) were *ex situ* analyzed by powder XRD and Mössbauer spectroscopy. It is found that PB exhibits a negative thermal expansion prior to the water release from its crystalline lattice. Above 300 °C, the decomposition is based on the release of cyanogen gas from the PB structure. At 370 °C, a cubic iron cyanide compound is formed, while at higher temperatures several iron carbides were found. The subsequent thermal treatment of these carbides leads to the formation of metallic iron and graphite.
[doi:10.1017/S0885715617000471]

Key words: solid-state thermal decomposition, Prussian blue, iron carbides

I. INTRODUCTION

Thermally induced solid-state synthesis is a common method to prepare powder materials; therefore understanding the thermal decomposition process of particular materials is crucial to optimize the synthesis of derived materials. Non-ambient X-ray powder diffraction (XRD) technique proved to be a very useful tool, which in combination with thermal analysis (thermogravimetry—TG and differential scanning calorimetry—DSC) allows us to elucidate the mechanism of the desired reactions.

Beyond its wide use as a pigment and histology stain, Prussian blue (PB) [iron(III) hexacyanoferrate, $Fe_4^{3+}[Fe^{2+}(CN)_6]_3 \cdot xH_2O$, $x = 14–16$] has been also used as a precursor material for preparation of iron oxides through solid-state thermal decomposition (Machala *et al.*, 2013; Kong *et al.*, 2014; Maeng *et al.*, 2015), and more recently it was used as a precursor for synthesis of iron carbides (Zakaria, 2016).

There are many factors to be considered when contemplating on the solid-state route to synthesize a nanopowder material: temperature, atmosphere, heating rate, particle size and shape of the precursor, mass of the sample, and even thickness of the sample; it is important as well whether the precursor is a powder or pressed pellet. Changing any of these factors can lead to a different product formation, or at least a change in the thermal behavior of the precursor material is expected.

In the case of PB, several studies confirmed the previous statements. When heated in air at temperatures above 300 °C, after the breakdown of the crystalline structure by releasing of $(CN)_2$, PB is completely transformed into iron oxides: typically a mixture of maghemite and hematite (Zakaria *et al.*, 2014), but in some cases also β-Fe_2O_3 (Machala *et al.*, 2013) or amorphous phase (Zboril *et al.*, 2004) are formed. On the other hand, when PB is heated in inert atmosphere or vacuum, at temperatures above 350 °C, the formation of metallic iron and cementite (Fe_3C) is expected. In the previous study, PB was heated in argon up to 1000 °C with a heating rate of 10 K min^{-1} (Aparicio *et al.*, 2012), it is observed that the formation of cementite and metallic iron does not occur directly, but through four steps: dehydration of PB, formation of an iron cyanide compound with monoclinic structure, formation of several iron carbides polymorphs (Fe_2C, Fe_7C_3, Fe_3C), and, lastly, formation of metallic iron and carbon. Metallic iron and carbon are secondary products, produced after the cementite thermal decomposition at temperatures higher than 800 °C.

In view of the above, a detailed study of the thermal decomposition of PB was carried out in inert atmosphere with a low heating rate. The variation of one parameter, heating rate, led to interesting changes in the PB structure at the beginning of its thermal decomposition. The initial structural changes of the PB crystalline lattice before its decomposition were witnessed by high-temperature (*in situ*) XRD. While after the thermal decomposition of PB, the formation of iron carbides was monitored *in situ* and *ex situ* by the XRD. As a result, the relation between the different forms of iron carbides as well as their thermal stability with the increase of temperature was observed.

[a]Author to whom correspondence should be addressed. Electronic mail: claudia.aparicio@upol.cz

II. EXPERIMENTAL

A. Starting material and sample preparation

PB (Sigma Aldrich) was used without further treatment as a starting material. Thermal analysis (TG/DSC) of PB was carried out using a thermal analyzer (STA 449 C Jupiter, Netzsch), which was coupled to mass spectrometer (QMS 403 Aëolos, Netzsch) to analyze the evolved gases (EGA) during the decomposition reaction.

PB powder (10 mg) was placed into an open alumina crucible. Then, it was heated up to 900 °C under argon atmosphere (gas flow 30 ml min^{-1}), with heating and cooling rates of 5 and −40 K min^{-1}, respectively. An additional set of PB samples were heated up to selected temperatures (190, 300, 370, 540, 680, and 790 °C). The resulting samples were labeled as PB190, PB300, PB370, PB540, PB680, PB790, and PB900, respectively.

B. Characterization techniques

XRD patterns were recorded at room temperature (RT) with a PANalytical X'Pert PRO MPD diffractometer in the Bragg-Brentano geometry, Co$K\alpha$ radiation (40 kV, 30 mA, $\lambda = 0.1789$ nm), equipped with an X'Celerator detector and programmable divergence and diffracted beam anti-scatter slits. Samples were placed on a zero-background Si slide, gently pressed and scanned with a step size of 0.017°, and 2θ scan range from 15° to 105°. Phase identification and Rietveld quantitative phase analysis were performed using PANalytical HighScore Plus software with PDF-4+ and ICSD databases.

Transmission ^{57}Fe Mössbauer spectroscopy was carried out in a constant acceleration mode using a ^{57}Co source in rhodium matrix at RT. The spectrometer was calibrated with an α-Fe foil. The spectra were folded and fitted by Lorentzian functions using the computer program CONFIT2000 (Žák and Jirásková, 2006).

C. High-temperature *in situ* XRD

Thermal decomposition of PB was studied from the structural point of view by *in situ* XRD. Diffraction patterns were collected using a PANalytical X'Pert PRO MPD diffractometer (Co$K\alpha$ radiation) in the Bragg–Brentano geometry, equipped with an X'Celerator high-speed detector and an Anton Paar XRK-900 reaction chamber. The powder sample was placed directly on a glass ceramic Macor holder (14 mm diameter, 0.5 mm deep). Data collection was carried out under nitrogen atmosphere (pressure 1 bar, gas flow rate 20 ml min^{-1}), with a heating rate of 5 K min^{-1} from RT up to 900 °C. The collection time of each XRD pattern was 10 min (0.12 s $step^{-1}$, step size of 0.017°, 2θ scan range from 15° to 105°).

III. RESULTS AND DISCUSSION

A. Characterization of PB

The purity of commercial PB was checked by XRD and ^{57}Fe Mössbauer spectroscopy. Both techniques showed that PB powder consisted of iron(III) hexacyanoferrate (PDF 01-073-0689) and a minor phase (~3%) identified as the mineral Jarosite [PDF 01-076-0629, $(K,Na)Fe_3(SO_4)_2(OH)_6$] (Aparicio *et al.*, 2012). In addition, energy dispersive spectroscopy (EDS) has been performed on the PB sample, confirming the presence of the elements Na, S, and K (Figure S1).

B. Decomposition of PB under argon atmosphere: TG/DSC analyses

Six differentiated steps can be resolved in the TG curve of PB from RT to 900 °C (Figure 1, Table I). In the same graph the DSC curve and the evolution of gases during the heating process are presented. Water release ($m/z = 18$) takes place from 55 to 300 °C (according to EGA), which corresponds well with the observed decrease in mass and a wide endothermic peak at 150 °C (steps I and II). Using this information, the amount of water molecules per unit cell was calculated to be five, a number lower than the theoretical value for PB structure. Because of the small amount of Jarosite impurity (~3%) in the PB sample, its contribution is neglected from calculation of water content.

The thermal decomposition of PB in argon atmosphere started above 350 °C (step III), with the release of cyanide groups (CN^-, $m/z = 26$), forming thereafter hydrogen cyanide HCN ($m/z = 27$) and cyanogen gas $(CN)_2$ ($m/z = 52$), and a small amount of carbon dioxide (CO_2) ($m/z = 44$) according to the EGA results (Figure S2). It is reflected by the two small downward peaks in DSC (endo-effect) at 330 and 360 °C.

In contrast, the mass decrease in the other steps (IV–VI) is accompanied by the release of nitrogen (N_2, $m/z = 28$) and probably also a small amount of CO_2, during the formation of iron carbides above 400 °C (see the next section). Given that m/z could be assign either to N_2 or CO, one cannot rule out the presence of small amount of CO. In this particular case, the presence of the $m/z = 14$ (N), which is identified as

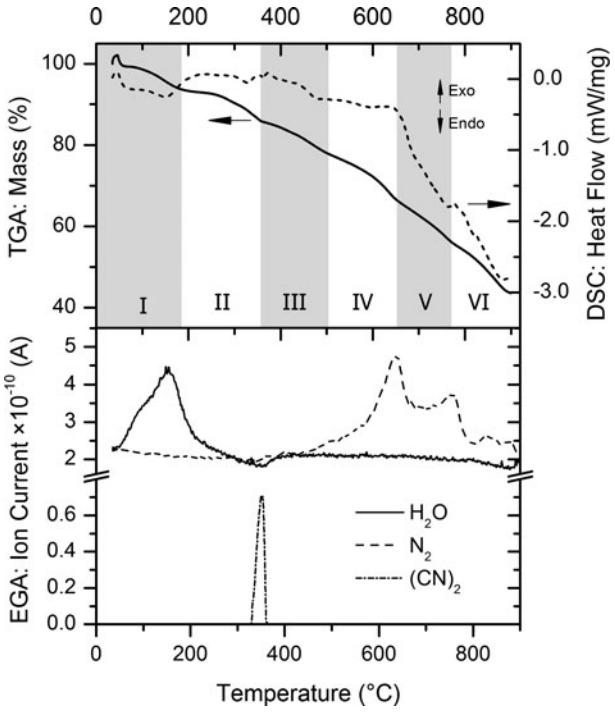

Figure 1. TGA, DSC, and EGA graphs of PB treated under argon atmosphere with a heating rate of 5 K min^{-1}. Roman numbers indicate the different steps of the decomposition.

https://doi.org/10.1017/S0885715617000471 Published online by Cambridge University Press

TABLE I. Mass loss estimated from TG curve for PB sample heated up to 900 °C in Ar.

Step	Temperature range (°C)	Mass loss (%)
I	35–189	−6.39
II	189–361	−7.85
III	361–505	−7.96
IV	505–649	−11.01
V	649–775	−10.98
VI	775–899	−12.19
	Total:	−56.39

the fragment of the molecular ion N_2, besides it have the same emission profile as $m/z = 28$ (Figure S2). From the previous discussion, it can thus be concluded that $m/z = 28$ is more likely to be assigned to N_2, and the CO contribution might be minimal.

C. Thermal behavior of PB under Ar atmosphere: *ex situ* XRD and Mössbauer spectroscopy

The phase composition of the PB samples thermally treated up to selected temperatures was variable, showing clearly not only the thermal decomposition of initial PB, but also the formation of iron carbides and their subsequent decomposition (Figure S3).

At 190 °C, a structurally unchanged PB and traces of Jarosite were observed, but at 300 °C PB becomes dehydrated, still preserving its crystalline character. Above 350 °C, PB decomposition has started; in sample PB370 were detected mainly non-transformed PB and an iron cyanide compound, additionally minor organic phases were identified (urea and malic acid). The formation of the aforementioned organic phases from PB (e.g. urea) has been reported earlier during thermal wet decomposition under inert atmosphere by Ruiz-Bermejo *et al.* (2009).

The formed iron cyanide compound match the PDF card 01-075-023, belonging to a Cu(II)–Fe(II) cyanide compound with a cubic structure (space group $F\bar{4}3m$). It is known, that most of the ferrocyanide compounds with the structure $M_2[Fe(CN)_6]$ crystallize in the cubic system, and can be indexed either with the space groups $F432$, $F\bar{4}3m$, or $Fm\bar{3}m$ (Ratuszna *et al.*, 1995), some examples of these cubic ferrocyanides are displayed in Figure S4 and the details are listed in Table S1. Other clue about the structure of this iron cyanide compound is given by the Mössbauer spectrum of the sample PB370 (Figure 2(a), Table II). In the spectrum, spectral components were identified (L1, D2) corresponding to undecomposed PB, the high value of quadrupole splitting (QS) can be related to strain in the PB lattice (Samain *et al.*, 2013). Sub-spectra L2 (singlet) and D1 (doublet) correspond to Fe^{2+} cations with low-spin and high-spin states, respectively. The presence of the singlet with a small isomer shift (IS = −0.09 mm s^{-1}) close to zero and absence of a QS, is a clear indicator of a highly symmetric site typical for cubic structures with fcc arrangement, where the Fe^{2+} is six-coordinated. The doublet (IS = 1.12 mm s^{-1}, QS = 1.47 mm s^{-1}), represent a Fe^{2+} cation with high-spin state. Then, both sub-spectral components can be assigned to the formed iron cyanide compound, where the values of the IS and QS are close to the ones measured in a pure sample of ferrous ferrocyanide (Hu and Jiang, 2011). It can be concluded that the formed compound is likely the iron(II) hexacyanoferrate (II) ($Fe_2[Fe(CN)_6]$), also known as Berlin white (BW). Finally, the provenance of the singlet (L3) with a broad linewidth will be explained below.

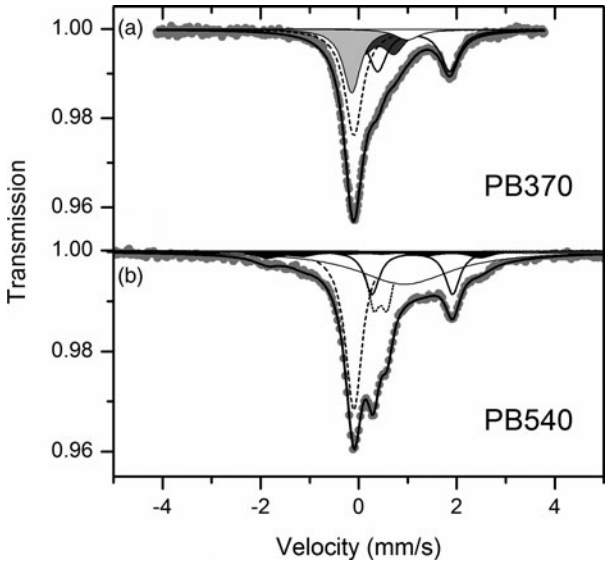

Figure 2. Room-temperature Mössbauer spectra of samples PB370 (a) and PB540 (b). PB (gray and dark gray subspectra), BW (white doublet and dashed singlet), Fe_2C (black sextet).

The formation of BW differs from the previous study, where a monoclinic iron cyanide structure was identified (Aparicio *et al.*, 2012); however, it agrees with other study performed in argon atmosphere (Allen and Bonnette, 1974). It is suggested that the reason of such disagreement might be the different heating rate of 10 vs. 5 K min^{-1} in this study, as this can be compared with the diffraction patterns from PB samples taken after the dehydration steps at the beginning of the PB transformation (step III, at 400 and 380 °C for samples heated under argon with 10 and 5 K min^{-1}, respectively) in Figure S5, where the diffraction patterns are significantly different.

At 540 °C, all PB has been transformed into BW, and also simultaneously started the formation of iron carbides: hexagonal ($Fe_{2+x}C$, $P6_322$) and orthorhombic (Fe_2C, $Pbcn$) forms. Minor phases oxydiacetic acid and urea has been also identified. From the Mössbauer spectrum (Figure 2(b), Table II) BW was identified (D2, L1), where the doublet has a higher value of QS, denoting a deformation of the octahedral site of ferrous ions. It was not possible to assign the doublet D1 (ferric ions most probably in octahedral coordination) to any compound identified in the XRD pattern. The singlet L2, with a very wide linewidth, has a similar isomer shift to singlet L3 in sample PB370. It could reflect the arrangement of iron cations prior to the formation of iron carbides, being in accordance with the poor crystallinity of iron carbides observed in the respective XRD pattern. The presence of a sextet with small subspectral area (7.3%) is ascribed to crystalline Fe_2C.

In sample PB680, it is observed that the formation of Eckstrom-Adcock carbide (Fe_7C_3, $P6_3mc$) along with other iron carbides. At higher temperatures, the samples typically contain different iron carbides: in sample PB790 were identified Fe_7C_3, Hägg carbide (Fe_5C_2, $C12/c1$), cementite (Fe_3C, $Pnma$), and a small amount of $K_4[Fe(CN)_6]$. The formation

https://doi.org/10.1017/S0885715617000471 Published online by Cambridge University Press

TABLE II. Mössbauer parameters obtained from the fit of spectra for samples PB370 and PB540 heated under argon atmosphere.

Sample	Sub-spectrum assignment	*IS* (mm s^{-1})	*QS* (mm s^{-1})	*W* (mm s^{-1})	B_{hf} (T)	Area (%)
PB370						
D1	BW Fe^{2+} (HS)	1.12	1.47	0.44	–	26.5
D2	PB Fe^{3+} (HS)	0.41	0.63	0.50	–	16.1
L1	PB Fe^{2+} (LS)	−0.14	–	0.42	–	19.4
L2	BW Fe^{2+} (LS)	−0.10	–	0.44	–	33.3
L3	Fe^{2+} (HS)	0.99	–	0.60	–	4.7
PB540						
S1	Fe_2C	0.22	0.19	0.60	13.5	7.3
D1	Fe^{3+} (HS)	0.44	0.27	0.30	–	14.3
D2	BW Fe^{2+} (HS)	1.09	1.64	0.37	–	13.2
L1	BW Fe^{2+} (LS)	−0.10	–	0.41	–	29.6
L2	Fe^{2+} (HS)	0.93	–	2.35	–	35.6

IS, isomer shift; *QS*, quadrupole splitting; *W*, experimental line width; B_{hf}, magnetic hyperfine field; HS, high spin; LS, low spin; S, sextet; D, doublet; L, singlet.

of Fe_5C_2 was not observed at higher heating rates (Aparicio *et al.*, 2012). In sample PB900 the predominant phase is cementite, additionally, diffraction lines from metallic iron (α-Fe, $Im\bar{3}m$) were also present.

D. Thermal behavior of PB under nitrogen atmosphere: *in situ* XRD

The 43 XRD patterns collected during the high temperature measurements were categorized into six groups, corresponding to the steps observed in TG (Figure 1). Representative XRD patterns from each group are shown in Figure 3. Quantitative phase analysis was performed for all diffraction patterns using the Rietveld method, considering only the known phases and excluding the minor phases in the XRD patterns. Unit-cell of PB was refined using the Herren model with $Fm\bar{3}m$ space group (Herren *et al.*, 1980), and BW was refined using the Ratuszna and Juszczyk model with $F\bar{4}3m$ space group (Juszczyk *et al.*, 1994; Ratuszna *et al.*, 1995) for anhydrous forms of $M_2[Fe(CN)_6]$.

Below 300 °C, PB is not decomposed and the structure is preserved, but one can observe changes in the position of the main diffraction peaks in the XRD pattern (Figure S6). Up to 180 °C, reflections (*200*), (*220*), and (*400*) are shifted to the high-angle side with the increase in temperature, clearly indicating a negative thermal expansion (Matsuda *et al.*, 2009). On the contrary, a positive thermal expansion is observed above 180 °C. The observed negative thermal expansion can be related to dehydration of PB, as a result of a progressive contraction of the unit cell with the release of water molecules (Figure 4).

Figure 5 summarizes the course of PB transformation into BW, further decomposed into iron carbides, leading to the final products cementite, iron, and carbon; results which are comparable with those obtained when PB was heated under argon.

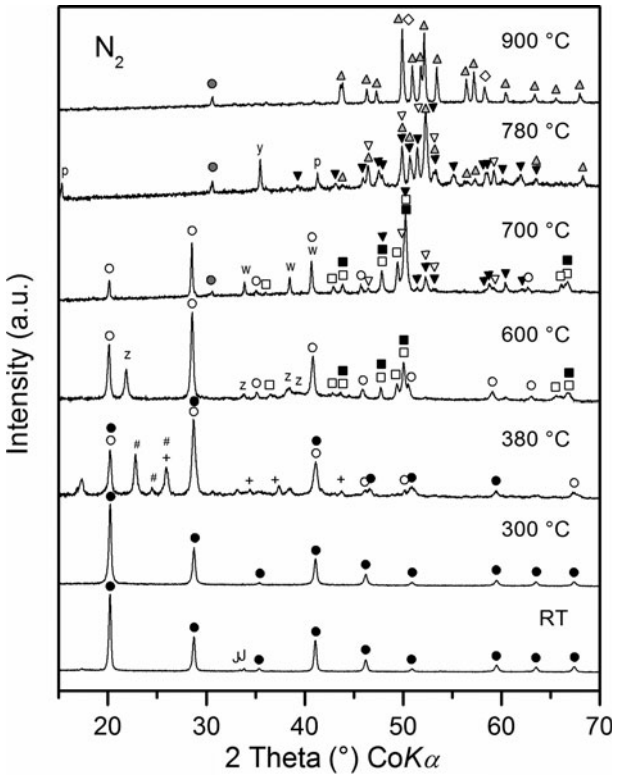

Figure 3. Selected XRD patterns from *in situ* measurements of PB heated under N_2. The symbols represent the identified phases: Jarosite (J), $Fe_4[Fe(CN)_6]_3$ (●), $Fe_2[Fe(CN)_6]$ (○), $Fe_{2+x}C$ (■), Fe_2C (□), Fe_7C_3 (▽), Fe_2C_5 (▼), Fe_3C (▲), γ-Fe^0 (◇), C (◉), Urea (+), Malic acid (#), 2-Naphthylamine-1-sulfonic acid (z), $Na_2(SO_3)$ (w), K_3N (p), NaCN (y).

E. Overall mechanism of thermal decomposition of PB and relationship between iron-carbide phases

The first step in the thermal decomposition of PB is dehydration. In the TG graph (Figure 1) the mass loss between

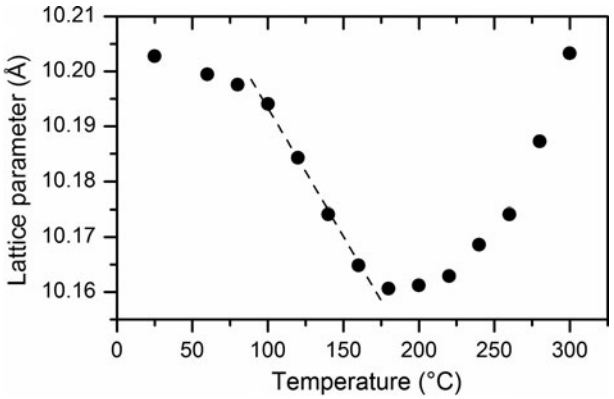

Figure 4. Temperature dependence of unit-cell parameters of PB showing negative thermal expansion. The dashed line is a guide to the eye.

https://doi.org/10.1017/S0885715617000471 Published online by Cambridge University Press

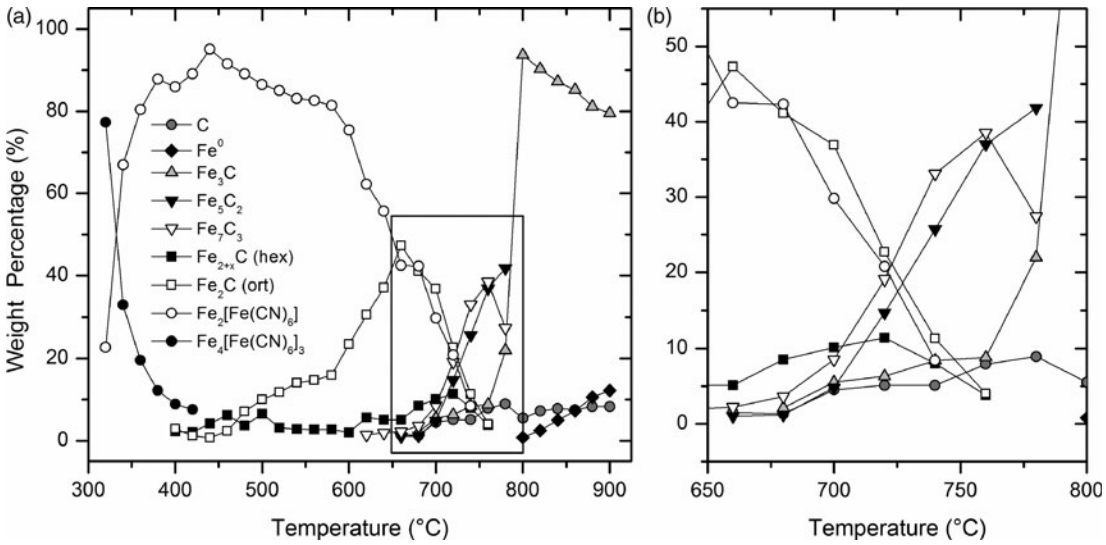

Figure 5. (a) Quantitative results of the Rietveld analysis of XRD patterns collected *in situ* during the thermal decomposition of PB under nitrogen atmosphere. (b) Close-up view of the central region of the graph marked with a rectangle in (a).

35 and 189 °C corresponds to the release of 3.5 uncoordinated water molecules from the PB structure ($\Delta m_{th} = -6.39\%$). Then, a slight decrease of mass up to 300 °C, corresponds to the release of 1.5 coordinated water molecules ($\Delta m_{th} = -3.09\%$).

Between 300 and 420 °C, along with the release of $(CN)^-$ groups from the dehydrated PB structure, PB is transformed into BW (Figure 5), according to the following reaction:

$$Fe_4[Fe(CN)_6]_3 \rightarrow 7/3Fe_2[Fe(CN)_6] + 2(CN)_2. \quad (1)$$

Figure 5 shows that orthorhombic Fe_2C and hexagonal $Fe_{2+x}C$ ($0 \le x \le 0.33$) are the first iron carbides formed up to 580 °C, followed by a steady increase of the amount of Fe_2C between 580 and 660 °C, thus indicating a faster decomposition of BW. At 620 °C, hexagonal iron carbide Fe_7C_3 is formed. The process can be explained by the following equations:

$$7Fe_2C \rightarrow 2Fe_7C_3 + C, \quad (2)$$

$$3Fe_{2+x}C \rightarrow Fe_7C_3. \quad (3)$$

Between 660 and 760 °C, the iron carbide Fe_5C_2 has been formed, and its weight percentage increases steeply at the same rate as Fe_7C_3. The weight percentage of both iron carbides increases (Fe_5C_2 and Fe_7C_3) at the same time that the weight percentage of Fe_2C decreases, suggesting a transformation of the primary iron carbide. Minor phases Fe_3C and C are also present. The possible relation between these carbides can be expressed by:

$$6Fe_2C \rightarrow Fe_7C_3 + Fe_5C_2 + C, \quad (4)$$

$$4Fe_2C \rightarrow Fe_5C_2 + Fe_3C + C. \quad (5)$$

A decrease in Fe_7C_3 (−11 wt%) is observed between 760 and 780 °C. At the same time, the weight percentage of Fe_5C_2 and Fe_3C increased by 5 and 13%, respectively. The sharp rise in Fe_3C weight percentage might be explained by the equations:

$$3Fe_7C_3 \rightarrow 7Fe_3C + 2C, \quad (6)$$

$$3Fe_5C_2 \rightarrow 5Fe_3C + C. \quad (7)$$

Equation (7) has been proposed earlier by Iguchi *et al.* (2004) and Herranz *et al.* (2006). It is also known that formation of cementite occurs at temperatures higher than 480 °C and that Fe_5C_2 always precedes Fe_3C formation (Cohn and Hofer, 1953).

Above 800 °C, the phase composition consists of Fe_3C, γ-Fe, and C. It is obvious from Figure 5 that the decrease in weight percentage of Fe_3C corresponds to a formation of γ-Fe and C ($3\ Fe_3C \rightarrow 3\ Fe + C$), because of the instability of cementite at temperatures higher than 700 °C (Iguchi *et al.*, 2004; Chaira *et al.*, 2007).

The observed transformations between carbides agree with the known fact that the stability of iron carbides increases when the carbon content decreases: $Fe_2C < Fe_{2.2-2.4}C < Fe_5C_2 < Fe_3C$ (Le Caer *et al.*, 1982; Jung and Thomson, 1992).

Taking into account the provided information by TG/EGA and XRD, one can summarize the overall decomposition mechanism of PB in inert atmosphere by Eq. (8). In this equation, nitrogen was included. Although its provenance is not well understood, it was released during the transformation of iron carbides (Figure 1): Fe_2C to Fe_5C_2 and Fe_7C_3 (642 °C), Fe_7C_3 to Fe_3C (763 °C), and Fe_3C to Fe (842 °C). Such as nitrogen release has been witnessed before in other studies during the thermal decomposition of insoluble PB (Allen and Bonnette, 1974), soluble PB (Chamberlain and Greene, 1963), and other hexacyanoferrates (Gallagher and Prescott, 1970) in inert atmosphere or vacuum. In those cases, the nitrogen was detected above 400 °C in the case of the PB, and above 600 °C in the case of the other hexacyanoferrates. Additionally, as in the present study, the final decomposition products of the aforementioned compounds are Fe_3C, Fe, and C. These studies only mention the final products, but not the intermediate iron carbides, and they claim thermal decomposition follow the route: ferrocyanide → $Fe(CN)_2$ → Fe_3C, Fe, C. Other reasons supporting the evolution of nitrogen is the fact that the main products of PB decomposition are iron carbides and not iron nitrides as proved by EDS analysis

https://doi.org/10.1017/S0885715617000471 Published online by Cambridge University Press

(Figure S1). Other minor compounds containing nitrogen has been identified from XRD (Figure 2 and S1), but they also contain elements from the impurities of the precursor material (K, Na, and S) as proved from EDS analysis (Figure S1).

$$Fe_4[Fe(CN)_6]_3 \cdot 5H_2O \rightarrow 2Fe_3C + Fe + 2C + 7(CN)_2 + 2N_2 + 5H_2O. \quad (8)$$

The theoretical mass loss is −53.74%, as calculated from Eq. (8), which slightly differs from the experimentally observed mass loss of −56.39%. The reason for the differences could be attributed to the minor impurities in the initial PB.

IV. CONCLUSION

PB decomposes when heated above 300 °C under inert atmosphere with a low heating rate. Dehydration of PB occurs at about 150 °C, followed by degradation of the structure leading to release of cyanogen gas $(CN)_2$, thus leading to a transformation of PB to the cubic iron(II) hexacyanoferrate(II), and finally to the breakdown of the formed cubic structure. The products formed after decomposition of PB are mainly iron carbides. Initially, Fe_2C (hexagonal and orthorhombic) is formed and then transformed to other crystalline forms of iron carbides: Fe_5C_2, Fe_7C_3, and Fe_3C. A small amount of iron (α- or γ-Fe^0) is also formed as a result of the decomposition of cementite (Fe_3C) at temperatures higher than 800 °C in inert atmospheres.

SUPPLEMENTARY MATERIAL

The supplementary material for this article can be found at https://doi.org/10.1017/S0885715617000471

ACKNOWLEDGEMENTS

The authors gratefully acknowledge the financial support provided by the Ministry of Education, Youth and Sports of the Czech Republic (LO1305).

Allen, J. F. and Bonnette, A. K. (**1974**). "Thermal decomposition of Prussian blue: isotopic labeling with Mössbauer-inactive Fe-56," J. Inorg. Nucl. Chem. **36**, 1011–1016.

Aparicio, C., Machala, L., and Marusak, Z. (**2012**). "Thermal decomposition of Prussian blue under inert atmosphere," J. Therm. Anal. Calorim. **110**, 661–669.

Chaira, D., Sangal, S., and Mishra, B. K. (**2007**). "Synthesis of aluminium–cementite metal matrix composite by mechanical alloying," Mater. Manuf. Process. **22**, 492–496.

Chamberlain, M. and Greene, A. (**1963**). "Differential thermal analysis on some cyano and cyanonitrosyl ion complexes," J. Inorg. Nucl. Chem. **25**, 1471–1475.

Cohn, E. M. and Hofer, L. J. E. (**1953**). "Some thermal reactions of the higher iron carbides," J. Chem. Phys. **21**, 354–359.

Gallagher, P. K. and Prescott, B. (**1970**). "Further studies of the thermal decomposition of Europium Hexacyanoferrate (III) and ammonium Europium Hexacyanoferrate(II)," Inorg. Chem. **9**(11), 2510–2512.

Herranz, T., Rojas, S., Pérez-Alonso, F. J., Ojeda, M., Terreros, P., and Fierro, J. L. G. (**2006**). "Genesis of iron carbides and their role in the synthesis of hydrocarbons from synthesis gas," J. Catal. **243**, 199–211.

Herren, F., Fischer, P., Ludi, A., and Hälg, W. (**1980**). "Neutron diffraction study of Prussian blue, $Fe_4[Fe(CN)6]3_xH_20$. Location of water molecules and long-range magnetic order," Inorg. Chem. **19**, 956–959.

Hu, M. and Jiang, J. S. (**2011**). "Facile synthesis of air-stable Prussian white microtubes via hydrothermal method," Mater. Res. Bull., **46**, 702–707.

Iguchi, Y., Kouda, T., and Shibata, T. (**2004**). "Kinetics of decomposition and re-oxidation resistance of θ- and χ-Iron carbides at elevated temperatures and influence of their formation conditions," ISIJ Int. **44**, 243–249.

Jung, H. and Thomson, W. J. (**1992**). "Dynamic X-ray diffraction study of an unsupported iron catalyst in Fischer–Tropsch synthesis," J. Catal. **134**, 654–667.

Juszczyk, S., Johansson, C., Hanson, M., Ratuszna, A., and Małecki, G. (**1994**). "Structural and magnetic properties of $Me_2[Fe(CN)_6]$ compounds, where Me are 3d transition metals," J. Magn. Magn. Mater. **138**, 281–286.

Kong, B., Tang, J., Wu, Z., Wei, J., Wu, H., Wang, Y., Zheng, G., and Zhao, D. (**2014**). "Ultralight Mesoporous Magnetic Frameworks by Interfacial Assembly of Prussian Blue Nanocubes," Angew. Chem. Int. Ed. **53**, 2888–2892.

Le Caer, G., Dubois, J., Pijolat, M., Perrichon, V., and Brussi re, P. (**1982**). "Characterization by Mössbauer spectroscopy of iron carbides formed by Fischer–Tropsch synthesis," J. Phys. Chem. **86**, 4799–4808.

Machala, L., Zoppellaro, G., Tuček, J., Šafářová, K., Marušák, Z., Filip, J., Pechoušek, J., and Zbořil, R. (**2013**). "Thermal decomposition of Prussian blue microcrystals and nanocrystals – iron(III) oxide polymorphism control through reactant particle size," RSC Adv. **3**, 19591–19599.

Maeng, H. J., Kim, N., Lee, D. K., and Yu, H. (**2015**). "Synthesis of mesoporous iron oxide particles by using Prussian blue," Bull. Korean Chem. Soc. **36**, 1058–1060.

Matsuda, T., Kim, J. E., Ohoyama, K., and Moritimo, Y. (**2009**). "Universal thermal response of the Prussian blue lattice," Phys. Rev. B **79**, 172302.

Ratuszna, A., Juszczyk, S., and Małecki, G. (**1995**). "Crystal structure of the three-dimensional magnetic network of type $Me_k[Fe(CN)_6]_l \cdot mH_2O$, where Me=Cu, Ni, Co," Powder Diffr. **10**(4), 300–305.

Ruiz-Bermejo, M., Rogero, C., Menor-Salván, C., Osuna-Esteban, S., Martín-Gago, J., and Veintemillas-Verdaguer, S. (**2009**). "Thermal wet decomposition of Prussian blue: implications for prebiotic chemistry," Chem. Biodivers. **6**, 1309–1321.

Samain, L., Grandjean, F., Long, G. J., Martinetto, P., Bordet, P., and Strivay, D. (**2013**). "Relationship between the synthesis of Prussian blue pigments, their color, physical properties, and their behavior in paint layers," J. Phys. Chem. C **117**, 9693–9712.

Žák, T. and Jirásková, Y. (**2006**). "CONFIT: Mössbauer spectra fitting program," Surf. Interface Anal. **38**, 710–714.

Zakaria, M. B. (**2016**). "Nanostructuring of nanoporous iron carbide spheres via thermal degradation of triple-shelled Prussian blue hollow spheres for oxygen reduction reaction," RSC Adv. **6**, 10341–10351.

Zakaria, M. B., Hu, M., Hayashi, N., Tsujimoto, Y., Ishihara, S., Imura, M., Suzuki, N., Huang, Y., Sakka, Y., Ariga, K., Wu, K., and Yamauchi, Y. (**2014**). "Thermal conversion of hollow Prussian blue nanoparticles into nanoporous iron oxides with crystallized hematite phase," Eur. J. Inorg. Chem. **2014**, 1137–1141.

Zboril, R., Machala, L., Mashlan, M., and Sharma, V. (**2004**). "Iron(III) oxide nanoparticles in the thermally induced oxidative decomposition of Prussian blue, Fe4[Fe(CN)6]3," Cryst. Growth Des. **4**, 1317–1325.